JOURNAL OF MATERIALS SCIENCE 16 (1981) 676–686

Film thickness effects on craze micromechanics

TERENCE CHAN, ATHENE M. DONALD, EDWARD J. KRAMER
Department of Materials Science and Engineering and the Materials Science Centre, Cornell University, Ithaca, New York 14853, USA

Air crazes have been grown from indentor "crack" tips in polystyrene films of thicknesses 0.11, 0.57 and 1.2 μm. Quantitative transmission electron microscopy is used to measure craze thickness and fibril volume fraction profiles. From these, profiles of craze fibril extension ratio, $\lambda(x)$, craze surface displacement, $w(x)$, and craze surface stress, $S(x)$, have been computed. For all thicknesses of film, the $\lambda(x)$ profiles prove that the craze thickens by drawing more material into the fibrils from the craze–matrix interface, rather than by fibril creep. The form of $S(x)$ is also similar for all thicknesses of film, with a maximum at the craze tip and a minimum approximately half way along the craze. The extension ratio profiles also show a maximum at the craze tip. The midrib, which develops in the high stress region behind the craze tip as the craze propagates, has a value of λ comparable to that found at the stationary craze tip. When an isolated craze grows in an initially homogeneous stress field the midrib is observed to be of constant thickness. In contrast the midribs of crazes grown from crack tips decrease in thickness to a constant value with distance from the crack tip. All these observations are explained by the surface drawing mechanism of craze thickening. The computed values of λ and the fibril stress, σ_t, for the thinnest film, are significantly lower than for the thicker two films. These changes are attributed to the absence of plastic constraint in the thinnest film, which decreases the fibril true stress necessary for surface drawing.

1. Introduction

The preceding paper [1] outlined the marked changes that occur in the fibril microstructure of air crazes in PS thin films as the film thickness is decreased below 200 nm. The average fibril diameter increases from its value of 6 nm in bulk PS to ~ 60 nm in films as thin as 100 nm. In this paper we show that there is also a change in the micromechanics of the craze as the film thickness is decreased. Craze thickening via the surface drawing mechanism can take place at lower true fibril stresses when the plastic constraint in the thickness direction is relaxed as it is in the thinnest films.

2. Experimental procedure

Polystyrene (PS) films of various thicknesses were prepared on glass slides and characterized as described in the preceding paper [1]. While the films were on the slide, a Tukon microhardness tester was used to make indentation marks in the film. The indentation produced a diamond-shaped hole approximately 40 μm long and 5 μm wide in the PS film. The grid bars of the annealed copper grid were precoated with PS. The grid, which was 5 cm long by 1 cm wide with 1 mm by 1 mm grid squares, was placed over the film (on the glass slide) so that an indentor hole was located at the centre of each grid square, with the long axis of the indentation perpendicular to the long axis of the grid sheet. The grid sheet was then tacked to the film at its corners by applying small drops of PS–toluene solution. After allowing these drops to dry for about 3 h, the whole assembly was submerged in distilled water for an hour after which the copper grid and

 0022–2461/81/030676–11$03.10/0

attached PS film could be removed from the glass slide. The PS film was then completely bonded to the grid bars surrounding each grid square by briefly exposing the PS film to benzene vapour [2]. After the copper grid was strained in tension perpendicular to the long axis of the indentor holes, crazes initiated and grew from the tips of the indentor "cracks". As for the PS films with isolated crazes described in the previous paper, the plastic strain in the copper grid (there is negligible strain recovery in the copper) held the PS film under the final strain after the grid was removed from the strain frame. Individual grid squares with suitable crazes growing from the indentor crack could be selected and cut from the grid without perturbing the stress in the film over this square.

3. Analysis of craze micromechanics

The craze micromechanical parameters were determined from an overlapping series of transmission electron micrographs (TEM) taken along the craze length (defined as the x-direction) using the procedure developed by Lauterwasser and Kramer [2]. The measureable parameters were the craze thickness profile $T(x)$ which was measured directly from the TEM images and the craze fibril volume fraction profile $v_f(x)$ which was determined from quantitative measurements of the image contrast. The optical densities, ϕ, on the electron image plate of the solid film, a hole through the film (in this case the indentor hole was convenient) and the craze were measured with a microdensitometer. At each position along the craze the fibril volume fraction was then computed from the relation [2]

$$v_f = 1 - \frac{\ln(\phi \text{ craze}/\phi \text{ film})}{\ln(\phi \text{ hole}/\phi \text{ film})}. \quad (1)$$

The craze surface displacement profile $w(x)$ can then be computed as

$$w(x) = \frac{T(x)}{2}[1 - v_f(x)]. \quad (2)$$

The thickness of bulk polymer which fibrillates to form the craze i.e. the primordial craze thickness $T_0(x)$ is given by

$$T_0(x) = T(x) - 2w(x) \quad (3)$$

and the fibril extension ratio profile $\lambda(x)$, computed assuming no volume change in plastic deformation process of fibril formation, is

$$\lambda(x) = \frac{1}{v_f(x)} = \frac{T(x)}{T_0(x)}. \quad (4)$$

Once $w(x)$ is known, it is possible to calculate the surface self stress profile $\Delta S(x)$, the set of stresses that would have to act on the craze matrix interface to maintain the observed $w(x)$ profile in the absence of any applied stress. Although a number of methods are available [3], a Fourier transform procedure due to Sneddon [4] is most convenient to compute $\Delta S(x)$

$$\Delta S(x) = \frac{2}{\pi}\int_0^\infty \bar{p}(\xi)\cos(x\xi)\,d\xi \quad (5)$$

where

$$\bar{p}(\xi) = \frac{\xi E}{2}\int_0^a w(x)\cos(\xi x)\,dx \quad (6)$$

where a is the distance between the centre of the indentor hole and the tip of one of the crazes and E is Young's modulus of the undeformed polymer. The total stress on the craze surface can be found by superposing the applied tensile stress σ_∞ acting perpendicular to the craze so that

$$S(x) = \Delta S(x) + \sigma_\infty. \quad (7)$$

In the present instance although the craze surface displacement can be measured, the surface displacements of the indentor crack are also needed. Since we anticipate from results on isolated crazes [2] that the stresses on the craze surface do not change more than 30% over the craze length, we estimate the crack surface displacements from those of the Dugdale model [5–7, 3], which assume that the stress which acts over the craze surface is a constant σ_y. The singularities caused by σ_∞ and $S(x)$ cancel and the following equation must hold

$$\int S\,d\beta = \frac{\pi}{2}\sigma_\infty \quad (8)$$

where $\beta \equiv \arccos(x/a)$. For the Dugdale model

$$\sigma_y = \frac{\pi\sigma_\infty}{2\beta_c} = \frac{\int S\,d\beta}{\beta_c}. \quad (9)$$

Here $\beta_c = \arccos(a_0/a)$ and a_0 is the crack half length. The appropriate value of σ_y can be determined by measuring σ_∞, a and a_0. The Dugdale crack/craze displacements are given by [6]

$$w(x) = \frac{a\sigma_y}{\pi E}H(\beta, \beta_c) \quad (10)$$

where

$$H(\beta, \beta_c) = \cos\beta \ln\left[\frac{\sin^2(\beta_c - \beta)}{\sin^2(\beta_c + \beta)}\right] + \cos\beta_c \ln\left[\frac{(\sin\beta_c + \sin\beta)^2}{(\sin\beta_c - \sin\beta)^2}\right]. \quad (11)$$

Equation 10 is used to estimate the crack opening displacements and small adjustments to this $w(x)$ are made [7] so that it joins smoothly with the $w(x)$ measured in the region of the craze. Since these adjustments (and the initial approximation that the craze stress is constant) only appreciably affect the stress in the local vicinity just ahead of the crack tip [7], this procedure is rigorous as long as we confine our stress measurement to regions in the craze more than 20 μm from the crack tip. Because the region just ahead of the crack crazes irregularly in thick films due to prior plastic deformation produced by the indentor, this restriction would have to be made anyway.

4. Results

Crazes have been grown from indentor crack tips in PS films of 3 different thicknesses: 1.2, 0.57 and 0.11 μm. The thickness profiles $T(x)$ of these crazes are displayed in Fig. 1a to c, respectively.

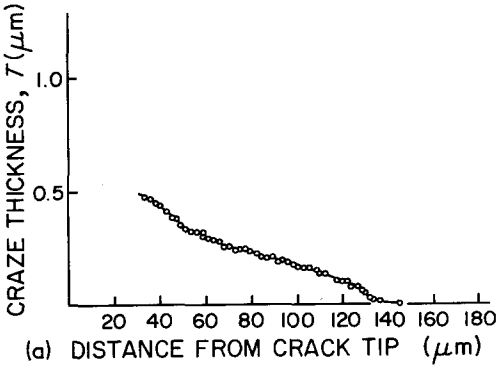

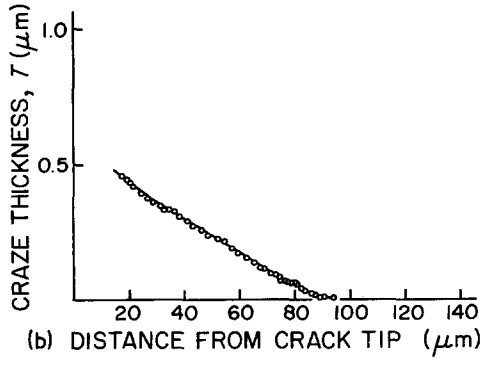

For the two thicker films there is a region, about 20 μm long, ahead of the crack tip which is incompletely fibrillated during craze growth. This region is shown in Fig. 2a to c for the three thicknesses. It arises due to the original indentation which pushes up a polymer "ridge" ahead of it, causing local thickening and orientation. The effect is most pronounced in Fig. 2a since the greatest volume of material must be displaced by the indentor in the thickest film. The craze thickness is not measured or defined in this region.

The extension ratio profile $\lambda(x)$ for the three crazes is shown in Fig. 3. The crazes in the two thicker films have very similar extension ratio profiles and these are qualitatively the same as the $\lambda(x)$ profile measured by Lauterwasser and Kramer [2] for an isolated craze in a 0.75 μm thick PS film. The extension ratio is constant at about 5 over most of the craze length but increases dramatically to very large values just behind the craze tip. These crazes show a midrib, a region of low v_f and high λ in the centre of the craze. The value of λ in the midrib, measured by local microdensitometry, is also shown in Fig. 3. In contrast the $\lambda(x)$ profile measured for the craze in the thinnest film is quite different. The extension ratio rises slowly from about 2 near the craze base to about 3 near the craze tip. Any complete explanation of the thick film/thin film craze transition must explain the much lower value of craze fibril strain in the thinnest film.

The craze surface displacement profile $w(x)$ from the irregular deformation zone to the craze

Figure 1 The thickness profile $T(x)$ for crazes in PS films of thicknesses (a) 1.2 μm, (b) 0.57 μm and (c) 0.11 μm.

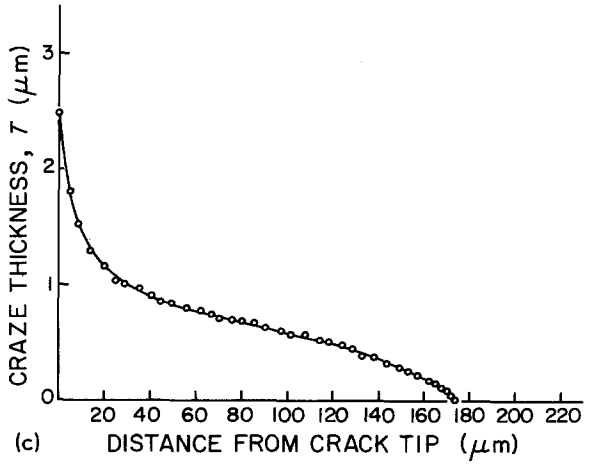

tip is computed from the $T(x)$ and $\lambda(x)$ data in Figs 1 and 3 and joined smoothly to the displacement profile in the crack computed from the Dugdale model. These profiles are shown in Fig. 4. Finally the Fourier transform method is used to compute the surface stress profiles $S(x)$ from the $w(x)$ data. These are displayed in Fig. 5.

5. Discussion

5.1. Stress profiles

The form of the craze surface stress profile is similar for each of the three films. The surface stress has a maximum at the craze tip and a minimum approximately halfway along the craze. In the 0.11 μm thick film where the surface displacements (and thus surface stresses) can be measured all the way to the crack tip the stress at the craze tip exceeds the final stress at the crack tip which has been relaxed by craze growth. The stress variation along the craze between the maximum (craze tip) and minimum (craze midsection) is approximately 30% for the two thicker films and about 50% for the thinnest films. The variation of 30% for the thicker films is similar to that observed by Lauterwasser and Kramer [2] for an isolated craze in a 0.75 μm thick PS film. Whereas for the isolated craze σ_∞ was about midway between the maximum and minimum stress, the effect of growing the craze from the starter crack is to raise both the maximum and minimum above σ_∞. The computed surface stress profile for one of the films is compared with that predicted by the Dugdale model in Fig. 6. Although the constant stress level predicted by the model is a reasonable average of the stresses over the craze length, it cannot predict the variation in stress observed along the craze length. Previous results of optical interference microscopy of crazes crack tips in PMMA have been interpreted as revealing craze displacement profiles in detailed agreement with the Dugdale model [9], but the much greater resolution of the present study casts some doubt on this claim. The displacement resolution of the optical technique is not good enough to reveal

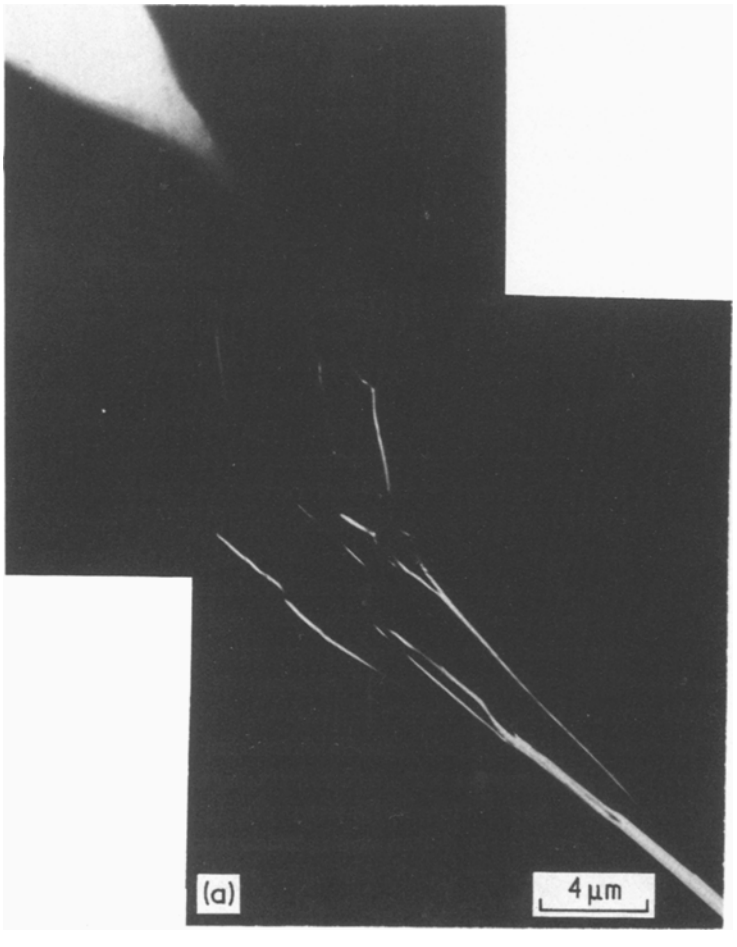

Figure 2 Irregular plastically deformed zone at the crack tip in (a) a 1.2 μm thick film (b) a 0.57 μm thick film and (c) a 0.11 μm thick film.

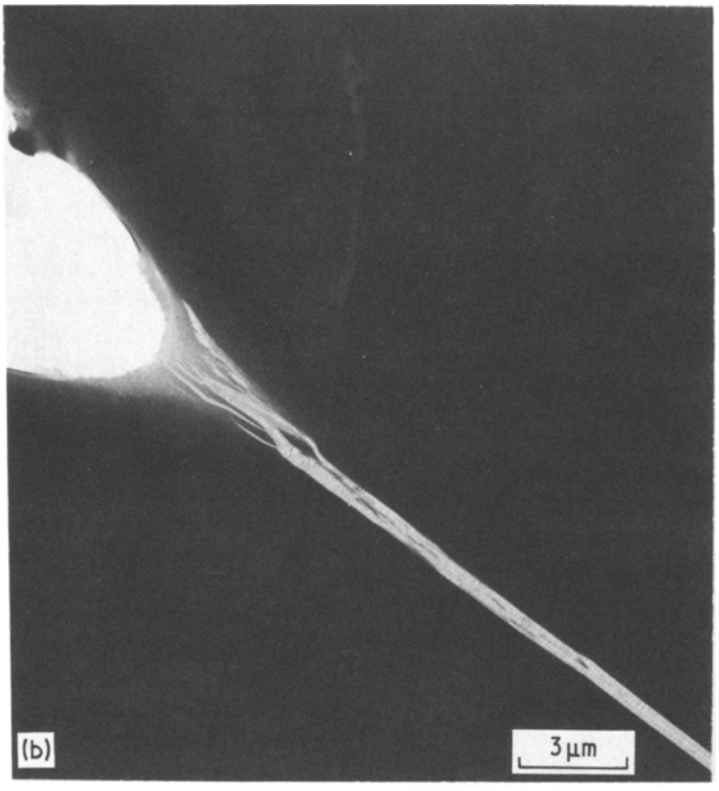

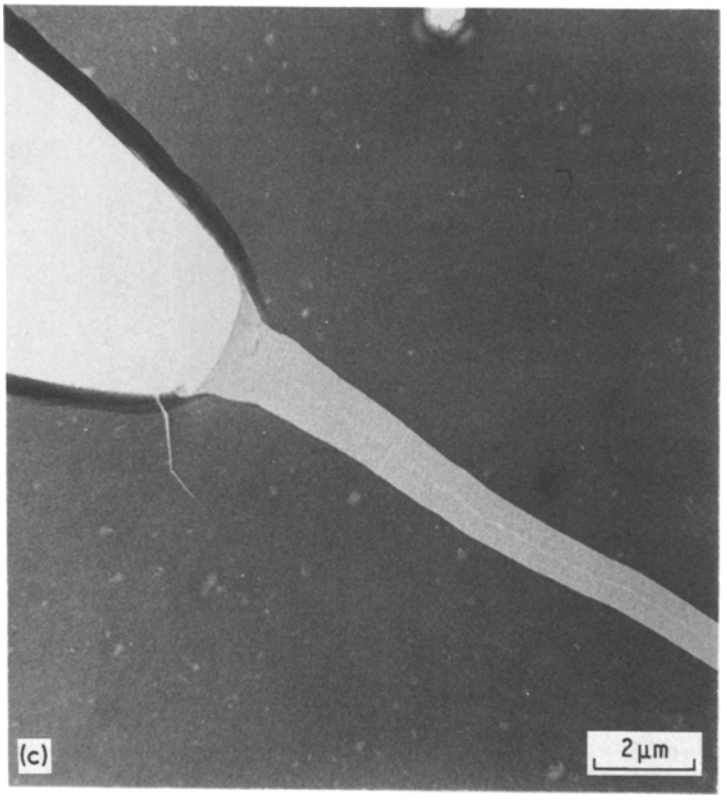

Figure 2 Continued.

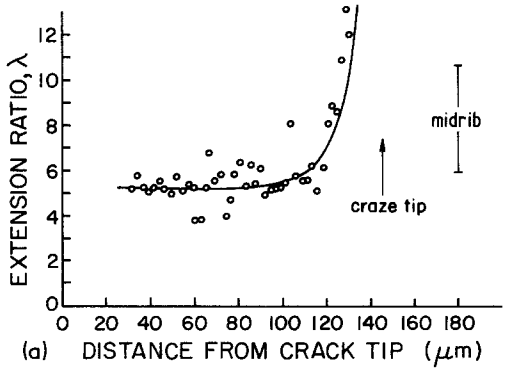

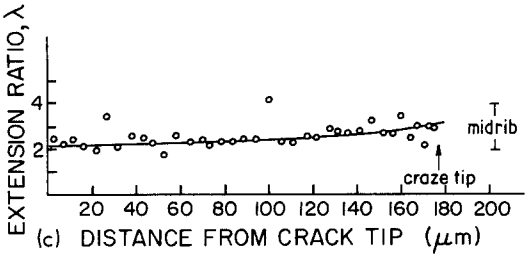

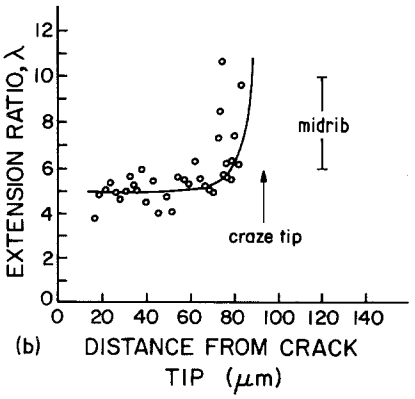

Figure 3 The extension ratio profile $\lambda(x)$ for crazes in films of thickness (a) 1.2 μm, (b) 0.57 μm and (c) 0.11 μm.

the precise form of the displacement profile $w(x)$ near the craze tip; these details are crucial in determining the stress concentration at the craze tip. Having pointed out the differences between the model and the experiment, however, one must also say that for many purposes such as computing the work done in the plastic zone the Dugdale model is a simple and quite satisfactory approximation. For example, computing G_{Ic}, the critical strain energy release rate, for a craze which moves rigidly with the crack tip, one finds [3, 6, 7]

$$G_{Ic} = 2 \int_0^{w_c} S(w)\, dw \qquad (12)$$

where w_c is the surface displacement at the crack tip. The G_{Ic} computed from the actual $S(x)$ and $w(x)$ profiles in Figs 4c and 5c is within 2% of the value estimated by the Dugdale model.

5.2. The mechanism of craze thickening

Two limiting mechanisms for craze thickening have been proposed. In the first [10], increases in craze thickness are supposed to take place by

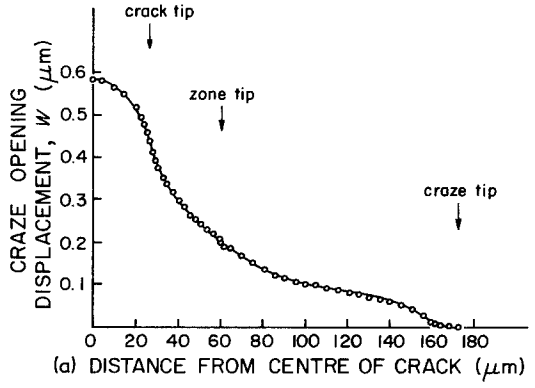

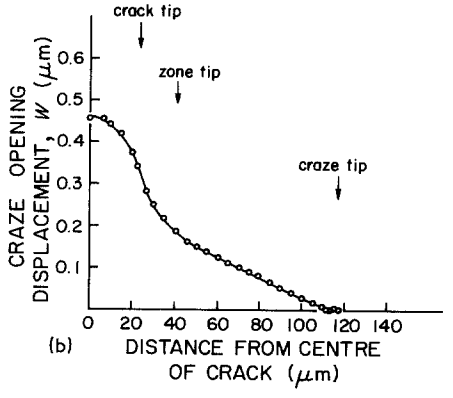

Figure 4 The craze surface displacement profile $w(x)$ for crazes in films of thickness (a) 1.2 μm, (b) 0.57 μm and (c) 0.11 μm.

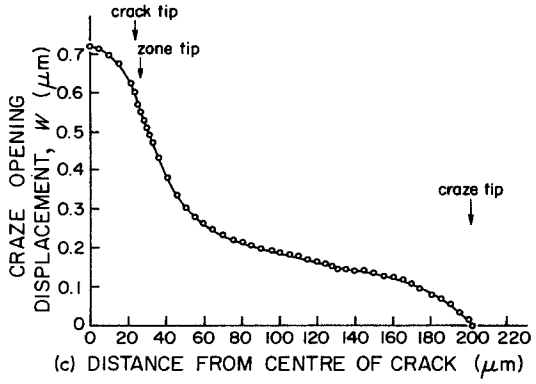

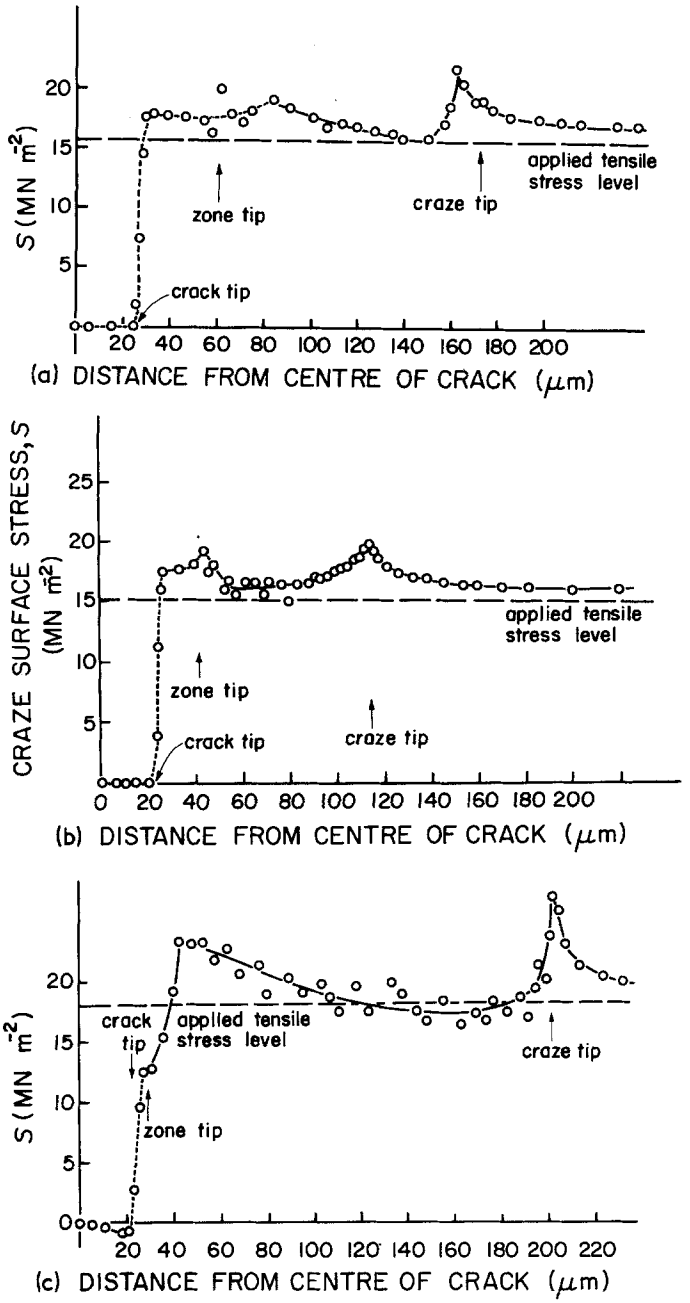

Figure 5 Surface stress profile $S(x)$ computed for crazes in films of thickness (a) 1.2 μm, (b) 0.57 μm and (c) 0.11 μm.

plastic creep of the craze fibrils after their formation at the craze tip. Fibril creep would be revealed in our experiments by a fibril extension ratio increasing with distance behind the craze tip (as the craze becomes thicker) and a primordial craze thickness T_0, corresponding to the original thickness of unoriented polymer which has fibrillated to form the craze and which is constant along the craze. Fig. 7 shows the $T_0(x)$ profile computed from Equation 3 for the crazes in the different films. From the marked increase in $T_0(x)$ with distance along the craze and the fact that the extension ratio profiles $\lambda(x)$ in all cases *decreases*, not increases, with distance behind the craze tip, we may conclude that fibril creep is not the dominant mechanism of craze thickening in any of our films.

Crazes may also thicken by drawing bulk

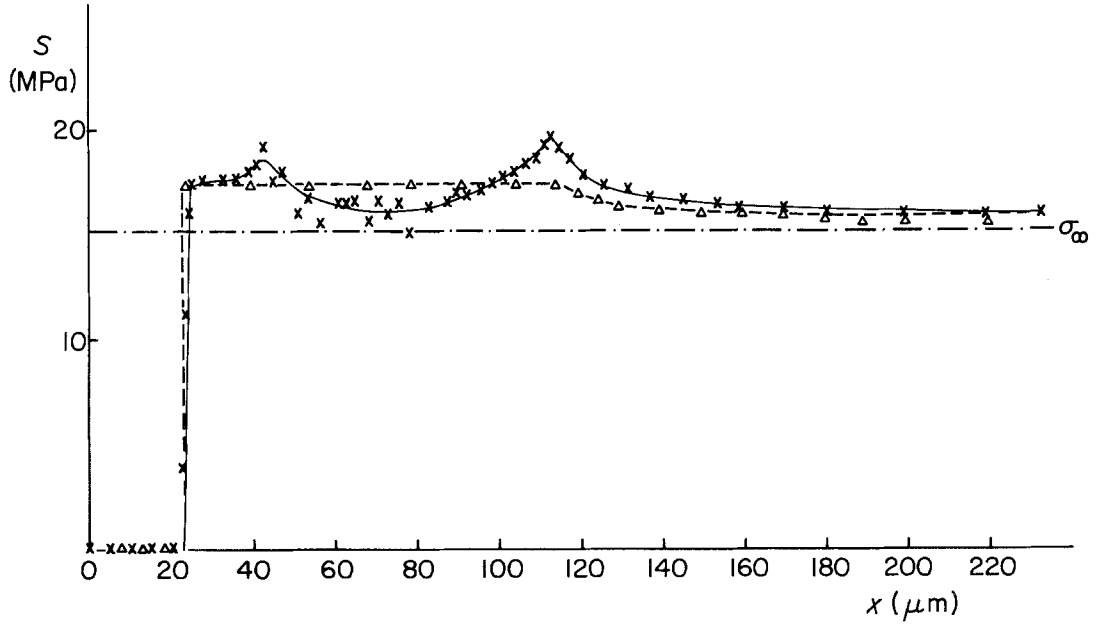

Figure 6 A comparison of the computed stress profile $S(x)$ for the 0.57 μm film with the profile predicted by the Dugdale model.

polymer into the fibrils at the craze–matrix interface. This mechanism (surface drawing) which is the analogue of neck propagation in fibre drawing, has been shown to be the dominant thickening mechanism for isolated air crazes in PS [2] and polycarbonate [11]. Whilst to a zero order approximation one might expect $\lambda(x)$ to be a constant for surface drawing. If there is a gradient in surface stress along the craze one logically expects fibrils drawn at higher stress (for example just behind the craze tip) to have higher λ's than those drawn at lower stresses. Lauterwasser and Kramer [2] showed that this assumption accounts well for the increase in $\lambda(x)$ just behind the craze tip in isolated PS air crazes and it would seem equally applicable to the present crazes grown from crack tips. The region of high λ behind the craze tip corresponds reasonably to the region of high S encountered there.

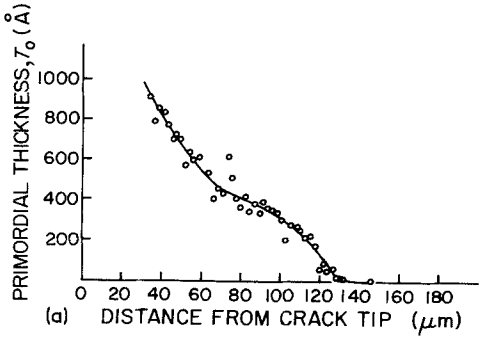

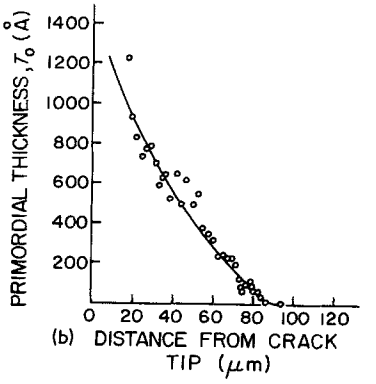

Figure 7 The primordial craze thickness profile $T_0(x)$, for crazes in films of thickness (a) 1.2 μm, (b) 0.57 μm and (c) 0.11 μm.

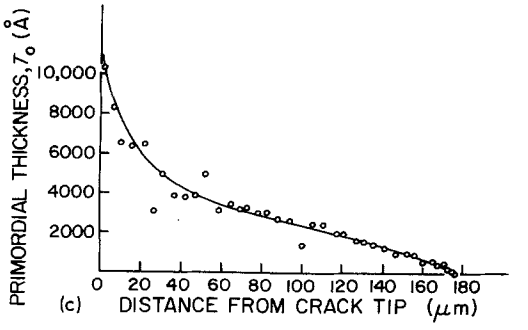

The surface drawing hypothesis also accounts for the presence of a midrib. As pointed out by Lauterwasser and Kramer as the craze propagates the region of high λ, formed behind the craze tip, remains as the high λ midrib in the centre of the mature craze. Fibrils drawn here become a high λ layer in the centre of the craze thickness. The thickness of the midrib in the isolated craze is approximately constant, which implies that the stress conditions behind the craze tip does not change markedly with craze growth. In the present experiments however, the craze tip grows in the initial inhomogeneous stress field ahead of the crack, so that when the craze tip is near the crack tip in the early stages of growth the overall stress level is high but it falls as the craze tip moves away from the crack. Under these conditions one might expect to find that the midrib of the craze is thickest in the region closest to the crack tip. Fig. 8 shows both the midrib thickness and the initial stress profile ahead of the crack tip for the craze in the 1.2 μm thick film; the crazes in other films show similar increases in midrib thickness near the crack tip. Clearly the inhomogeneous crack stress field produces just the effect on midrib thickness predicted by the surface drawing hypothesis.

The major, and only significant difference between the micromechanical behaviour of the craze in the thinnest film and those in the thicker films is the very much smaller value of λ in the craze in the thinnest film (Fig. 3c). This difference is attributed to the different conditions for fibril drawing from the craze–matrix interface in thin films versus thick films, and not from any intrinsic differences in PS properties in the various films. Referring to Fig. 9, we assume that the tensile stress σ_1 in the active drawing zone where the fibril meets the interface is of the order of the true stress σ_t in the fibrils. In addition there are lateral stresses σ_2 and σ_3. In the thickest film the stresses which develop due to plastic constraint normal and parallel to the film are equal so that $\sigma_2 \simeq \sigma_3$, but in the thin film no stress can develop normal to the film so that $\sigma_2 = 0$ and $\sigma_3 = \sigma_3$. Assuming that an equivalent yield stress σ_y in the fibril base must be maintained for drawing to continue, and using the Tresca criterion, one finds that the condition for drawing is

$$\sigma_t = \sigma_y + \sigma_2. \tag{13}$$

Thus for thin films with $\sigma_2 = 0$ drawing will occur at lower fibril true stresses than for thicker films where σ_2 is appreciable. The craze in the thinnest film does have much lower fibril stresses than the crazes in the thicker films [8]. In turn, given a certain strain hardening relationship between σ_t and λ for PS fibrils these lower σ_t's will result in lower λ's. If this idea is correct one would expect the same relationship between σ_t and λ to hold for the crazes in all three films. The true fibril stress is computed as a function of x from

$$\sigma_t(x) = \lambda(x)S(x). \tag{14}$$

Pairs of σ_t and λ values obtained from this equation are plotted in Fig. 10. Although the points for the thin film all lie at the low λ end of the line, it is clear that the same linear strain hardening behaviour is observed for all the films. Hence the strain hardening of the craze fibrils is an intrinsic property of PS and is not dependent on film thickness, and the ease of drawing of craze fibrils in thin film crazes must be related to the absence of lateral plastic constraint.

Given the difference in microstructure [1] and craze fibril extension ratios observed between thin and thick film crazes it is worth emphasizing once

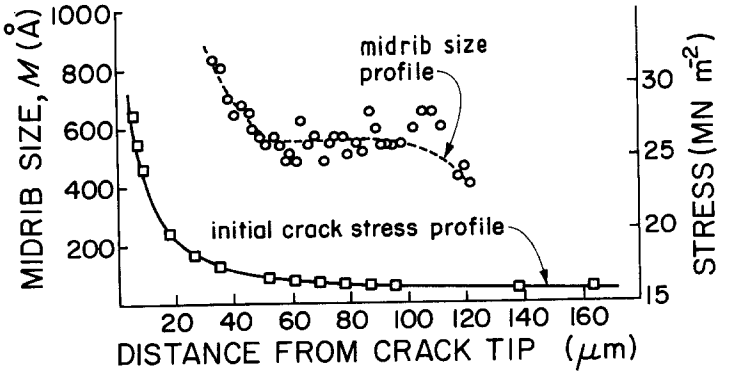

Figure 8 Profiles of the initial crack stress and the craze midrib width for the 1.2 μm thick film.

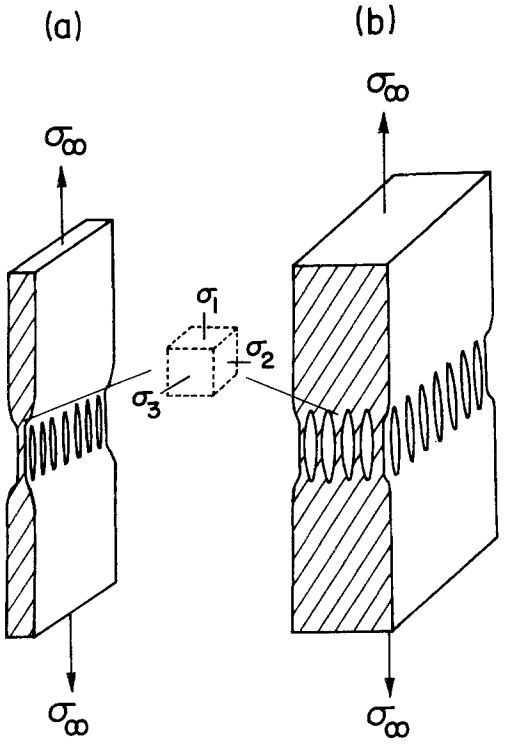

Figure 9 Schematic representation of fibril drawing conditions in "thin" and "thick" films.

more that for meaningful results, TEM investigations must use films which are thick enough to produce crazes that are typical of the crazes in bulk samples. For PS fortunately this transition occurs at thicknesses of about 150 nm, but in other materials e.g. (PMMA, PC etc.) it may well occur at much larger thicknesses.

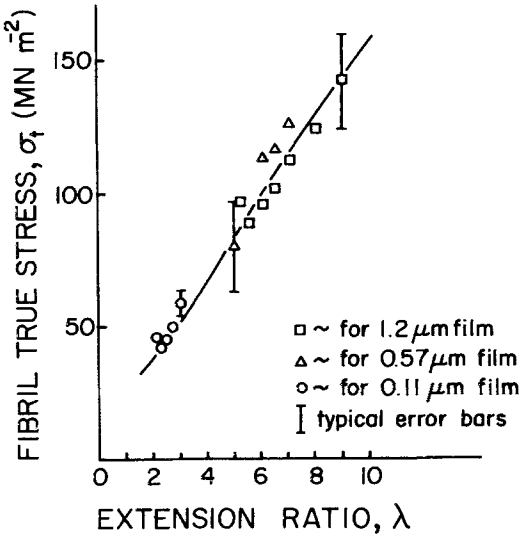

Figure 10 True fibril stress σ_t against extension ratio λ.

6. Conclusions

The following conclusions on microstructure and micromechanics of air crazes in polystyrene films can be drawn.

(1) Crazes in films thicker than 150 nm exhibit the same microstructure and micromechanics as crazes in bulk polystyrene. The fibril structure consists of roughly cylindrical fibrils, ~ 6 nm in diameter packed to a volume fraction between 0.15 and 0.25.

(2) Crazes in films thinner than 150 nm have a "perforated sheet" microstructure, with much larger diameter fibrils of up to 100 nm, and packed to much higher volume fractions, 0.33 to 0.5, than crazes in thicker films.

(3) All air crazes in polystyrene, regardless of film thickness, thicken by drawing new material from the craze–matrix interface into the fibrils, rather than by fibril creep.

(4) The mechanism of craze tip advance in the thickest film is the meniscus instability mechanism, which however can not operate in the thinnest films. In the thin film crazes the craze tip follows the advance of a surface groove plastic zone. This surface plastic zone also exists for crazes in thick films but has negligible influence on craze tip advance.

(5) The low extension ratios and high fibril volume fractions in crazes in the thinnest films are attributed to surface drawing of fibrils at lower true fibril stresses due to the lack of plastic constraint in the film thickness direction.

Acknowledgements

The financial support of this work by the US Army Research Office, Durham is gratefully acknowledged. The research also benefited from use of the facilities of the Cornell Materials Science Centre which is funded by the National Science Foundation. We appreciate the tutelage of Mr Vincent Wang in the art of bonding indented films and useful discussions with Dr Hugh R. Brown and Dr Nigel R. Farrar.

References

1. A. M. DONALD, T. CHAN and E. J. KRAMER, *J. Mater. Sci.* 16 (1981) 669.
2. B. D. LAUTERWASSER and E. J. KRAMER, *Phil. Mag.* 39 (1979) 469.
3. E. J. KRAMER, in "Developments in Polymer Fracture", Vol. 1, edited by E. H. Andrews (Applied Science, Barking, UK, 1979) Ch. 3.
4. I. N. SNEDDON, "Fourier Transforms" (McGraw-Hill, New York, 1951) pp. 395–430.

5. D. S. DUGDALE, *J. Mech. of Sol.* 8 (1960) 100.
6. J. N. GOODIER and F. A. FIELD, Proceedings of the International Conference on Fracture of Solids, edited by D. C. Drucker and J. J. Gilman, (Interscience, New York, 1963) p. 103.
7. G. I. HAHN and A. R. ROSENFIELD, *Acta Met.* 13 (1965) 293.
8. T. CHAN, MSc. Thesis, MSC Report Number 4178, Cornell University, 1979.
9. H. R. BROWN and I. N. WARD, *Polymer* 14 (1973) 469.
10. N. VERHEULPEN-HEYMANS and J. C. BAUWENS, *J. Mater. Sci.* 11 (1976) 7.
11. N. VERHEULPEN-HEYMANS, *Polymer* 20 (1979) 356.

Received 28 July and accepted 1 August 1980.